Check for updates

How to cite: *Angew. Chem. Int. Ed.* **2025**, *64*, e202501245
doi.org/10.1002/anie.202501245

Sensors **Hot Paper**

Readily Visualized Perfluorooctanoic Acid Detection Using a Small Molecule Chemosensor

Yu-Dong Yang, Qian Zhang, Xingchen Jin, Calvin V. Chau, Jian Yang, Graeme Henkelman, Xiaodong Chi,* Han-Yuan Gong,* Richard J. Hooley,* and Jonathan L. Sessler**

Dedicated to the memory of Sir Fraser Stoddart

Abstract: Mounting concerns regarding per-/poly-fluoroalkyl substances (PFAS) on human health are focusing attention on trace-level PFAS detection in aqueous environments. Here, we report a readily prepared small molecule, 2,6-bis(3,5-diethyl-*1H*-pyrrol-2-yl)pyridine (receptor **1**), that displays high binding affinities ($\log K_a = 4.9$–6.2) and produces a strong "turn-on" emission response when exposed to representative PFAS in hexanes. The hydrophobic nature of **1**, and its strong affinity for various PFAS, allowed hexanes solutions of **1** to be used as "turn-on" emission sensors for dilute aqueous solutions of long-chain ($\geq C_8$) PFAS under acidic conditions (pH 2) by liquid-phase extraction (LPE). In the case of perfluorooctanoic acid (PFOA), the response was rapid (under 10 min) and sensitive. Limits of detection (LOD) as low as 250 ppt were readily achievable by direct naked-eye observation. LOD as low as 40 and 100 ppt, respectively, could be reached for deionized and tap water solutions of PFOA using a smartphone color-scanning application. Little change in the sensitivity was seen in the presence of a range of inorganic and organic species that could act as potential interferants. Support for the present findings came from UV–vis absorbance, fluorescence, $^1H/^{19}F$ NMR spectroscopic analyses, density functional theory calculations, and single-crystal X-ray diffraction analyses.

Introduction

Per-/poly-fluoroalkyl substances (PFAS) have been widely employed in many consumer products and industrial processes since their discovery in 1950.[1] Their remarkable chemical stability, which has bestowed upon them the moniker "Forever Chemicals," has led to their accumulation in the environment and within living organisms. A growing body of research is heightening concerns that PFAS exposure may result in deleterious health outcomes, including liver damage, developmental retardation, fertility reduction, immune system inhibition, and an elevated risk of certain cancers.[2] The US Environmental Protection Agency (EPA) established guidelines for a number of PFAS contaminants, including 4 ppt for both perfluorooctanoic acid (PFOA) and perfluorooctane sulfonic acid (PFOS), in drinking water.[3,4] As a consequence, considerable efforts are being devoted to PFAS detection.[5,6] Nevertheless, there remains a need for new sensing approaches that could complement existing methods. As detailed below, we have now developed a small molecule receptor, 2,6-bis(3,5-diethyl-1H-pyrrol-2-yl)pyridine (**1**), that permits the real-time, high sensitivity (down to 40 ppt level) visualized detection of perfluorooctanoic acid (PFOA) through a liquid-phase extraction (LPE) approach (Scheme 1).

Over the past decades, a variety of techniques have been developed for PFAS detection, including liquid chromatography, mass spectrometry, surface-enhanced Raman scattering, surface plasmon resonance, fluorescence, and absorption spectroscopy.[7–10] Currently, liquid chromatography/tandem mass spectrometry (LC/MS/MS) is a preferred technique and is noted for its high specificity and sensitivity in detecting PFAS in aqueous environments.[11] However, its use requires specialized labs and trained personnel. Recently, the use of UV–vis absorbance or fluorescence emission spectral methods has attracted attention for PFAS detection as a result of their rapid, user-friendly, and cost-effective nature. A variety of sensor systems, including nanoparticles,[12] guanidinocalix[5]arenes,[13] β-cyclodextrin (β-CD) metal complexes,[14] metal–organic frameworks

[*] Y.-D. Yang, Q. Zhang, X. Jin, C. V. Chau, J. Yang, G. Henkelman, J. L. Sessler
Department of Chemistry, The University of Texas at Austin, 1105 East 24th Street, Stop A5300, Austin, TX 78712-1224, USA
E-mail: henkelman@utexas.edu
sessler@cm.utexas.edu

X. Chi
State Key Laboratory of Materials Processing and Die & Mold Technology, School of Materials Science and Engineering, Huazhong University of Science and Technology, Wuhan 430074, China
E-mail: xchi@hust.edu.cn

H.-Y. Gong
College of Chemistry, Beijing Normal University, Beijing 100875, China
E-mail: hanyuangong@bnu.edu.cn

R. J. Hooley
Department of Chemistry, University of California Riverside, Riverside, CA 92521, USA
E-mail: richard.hooley@ucr.edu

Additional supporting information can be found online in the Supporting Information section

© 2025 Wiley-VCH GmbH

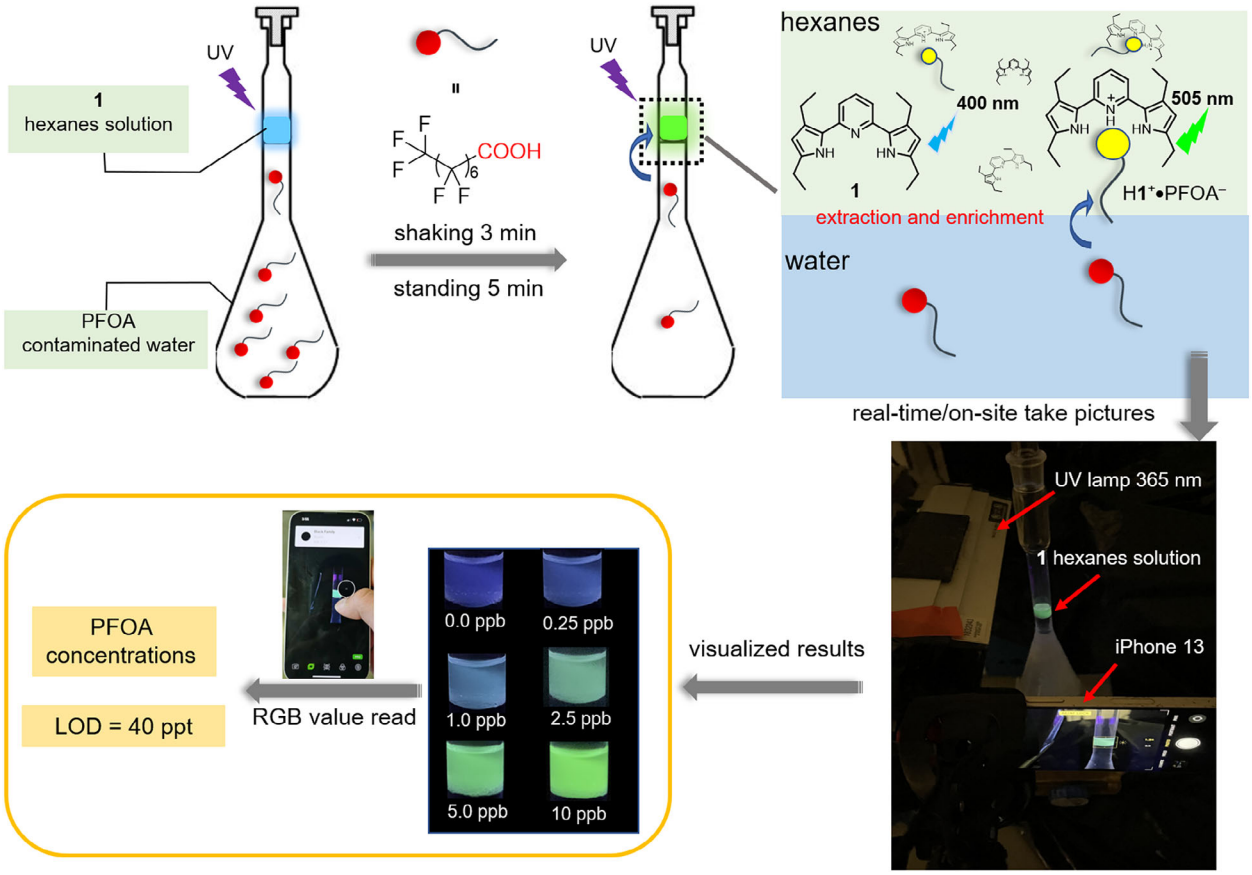

Scheme 1. Schematic representation of the present approach to the real-time visualized detection of PFOA using receptor **1**. The process involves extracting PFOA from water to a hexanes solution of **1**, resulting in the formation of a 1:1 complex, H**1**$^{+}$•PFOA^{-}. Complexation initiates a change in the emission of the hexanes solution from weak blue to intense yellow–green when irradiated with a commercially available UV lamp (365 nm). The colors can be directly observed by the naked eye or assessed by determining the red–green–blue (RGB) values using a smartphone color-scanning application. Both approaches allow quantification of the PFOA levels.

(MOFs),[15,16] amplifying fluorescent polymers (AFPs),[17,18] and several other materials,[19–28] have been employed in the latter context. The changes in colors resulting from the interaction between PFAS and appropriately designed sensors have kindled interest in developing naked-eye or smartphone-based visualized detection systems for PFAS.[14–16,18–21,29–37] Unfortunately, it has proved challenging to achieve the visualized detection of PFAS at ppt concentrations in aqueous environments. Moreover, the more promising systems reported to date are characterized by slow response times (>1 h), the need for complex operations, or necessitate extensive sensor preparation.[18,29] The development of PFAS sensors capable of high specificity and sensitivity while allowing for the real-time visualized detection of perfluorinated analytes in water remains a formidable challenge. This work was undertaken in an effort to address this challenge.

Results and Discussion

Preparation and Selection of Receptors

Dipyrrolylpyridines have been previously found to display readily discernible spectral responses when exposed to organic acids.[38] This led us to explore whether this class of open-chain expanded porphyrin precursors would act as sensors for PFAS. We postulated that the combination of hydrogen bond donor and acceptor sites within a cleft-like arrangement would allow the acid forms of PFAS to be bound with high affinity in organic media. This binding, in turn, was expected to alter the electronic features, producing ideally a "turn-on" emission-based response. Strong binding was also expected to drive the extraction-based transfer of PFAS into an organic phase containing a suitably optimized dipyrrolylpyridine receptor. This would allow their use as LPE-based sensors where the read-out element (the dipyrrolylpyridine) is contained in an organic phase, while the PFAS being monitored is initially present in the form of a dilute aqueous solution. To test this thinking, an effort was thus made to prepare several dipyrrolylpyridine derivatives. Our goal was to explore the PFAS recognition features, if any, of this class of putative receptors, assess structure–function relationships, and optimize the tradeoff between synthetic accessibility and anticipated PFAS sensing performance. Five dipyrrolylpyridines were designed to optimize cost, ease of preparation, and hydrophobicity for application in LPE detection methods. The compounds include 2,6-bis(3,5-diethyl-*1H*-pyrrol-2-yl)

© 2025 Wiley-VCH GmbH

15213773, 2025, 19, Downloaded from https://onlinelibrary.wiley.com/doi/10.1002/anie.202501245 by University Of Texas Libraries, Wiley Online Library on [21/05/2025]. See the Terms and Conditions (https://onlinelibrary.wiley.com/terms-and-conditions) on Wiley Online Library for rules of use; OA articles are governed by the applicable Creative Commons License

Table 1: Synthesis of receptors **1–5**.

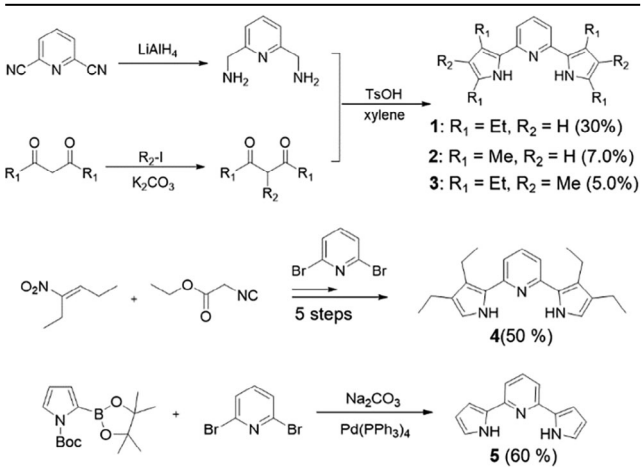

Targets	Reagents	Catalysts	Steps	Total Yield
1	Low-cost	TsOH	2	30%
2	Low-cost	TsOH	2	7.0%
3	Low-cost	TsOH	3	5.0%
4	High-cost	Noble metal	5	50%
5	Low-cost	Noble metal	1	60%

pyridine (**1**), 2,6-bis(3,5-dimethyl-*1H*-pyrrol-2-yl)pyridine (**2**), 2,6-bis(3,5-diethyl-4-methyl-*1H*-pyrrol-2-yl)pyridine (**3**), 2,6-bis(3,4-diethyl-1H-pyrrol-2-yl)pyridine (**4**), and 2,6-di-1H-pyrrol-2-ylpyridine (**5**).[38,39] These compounds were selected based on their favorable structural properties and practical synthesis from readily available starting materials. The preparation of these dipyrrolylpyridines involved three distinct synthetic routes, which are summarized in Table 1 and described in detail in the Supporting Information.

A comparison of the various syntheses revealed that receptor **5** benefited from the shortest synthesis and was obtained in the highest yield. We also found that receptor **1** could be prepared in high yield via a brief, cost-effective synthesis. Initial UV–vis absorbance studies revealed that all five receptors exhibited similar absorbance changes when exposed to PFOA in hexanes. In addition, noticeable emission color changes were seen under a commercially available laboratory UV lamp (365 nm). These involved a change from weak blue to blue-green in the case of receptor **5** and from weak blue to strong green in the case of receptors **1**–**3** and **4** (Figure S1). Unfortunately, receptor **2** showed water solubility, which made it unsuitable for use as an LPE-type PFAS sensor. Receptor **1** was thus chosen for detailed study given its low-cost preparation and attractive optical features.

Interactions Between 1 and PFAS

Initial studies of the interaction between **1** and PFOA were conducted by means of UV–vis absorbance and fluorescence spectroscopic titrations. Adding PFOA into a hexanes solution of **1** resulted in a decrease in the characteristic absorption of **1** (λ_{max} = 312 and 360 nm), as well as the simultaneous appearance of a peak at 346 nm and a strong broad peak at 474 nm. Companion fluorescence spectral titrations revealed a decrease in the emission peak of **1** (λ_{em} = 400 nm) and a simultaneous increase in the strong broad peak centered around 505 nm. A significant change in emission properties was observed when compound **1** interacted with PFOA, shifting the emission color from weak blue to intense yellow–green and resulting in a fivefold increase in relative quantum yield (Figure 1a–c). These spectral changes are attributed to the protonation of compound **1** by PFOA and the subsequent formation of the corresponding cation–anion complex, H**1**$^+$•PFOA$^-$. The protonation of **1** changes its highest occupied molecular orbital (HOMO) and lowest unoccupied molecular orbital (LUMO) energy levels, which explains the observed shifts in the UV–Vis and fluorescence spectra. This interpretation is further supported by density functional theory (DFT) calculations, as described below. Using a 1:1 binding model,[40,41] binding affinities were determined from independent fits of UV–vis and fluorescence spectral data, yielding values of LogK_a = 6.2 ± 0.1 and 6.1 ± 0.1, respectively. Subsequent NMR spectral studies in CD_3CN revealed shifts in both the ^{1}H NMR and ^{19}F NMR spectra consistent with the formation of an ion pair complex (H**1**$^+$•PFOA$^-$) stabilized by N-H-to-COO$^-$ hydrogen bonds. Specifically, the pyrrole NH (H_a) and CH (H_d) protons exhibited downfield shifts of 0.75 and 0.16 ppm, while the pyridine protons H_b and H_c shifted by 0.30 and 0.15 ppm, respectively. In the ^{19}F NMR spectrum, the F_2 and F_3 signals shifted downfield by 1.7 and 0.33 ppm (Figure 1e). These spectral changes are taken as evidence of strong hydrogen bonding and electrostatic interactions within the ion pair. Support for this suggestion came from single crystal X-ray diffraction analyses and DFT calculations (vide infra).

UV–vis and fluorescence spectral titrations were also performed between **1** and other fluorinated species, including trifluoroacetic acid (TFA), perfluorobutanoic acid (PFBA), perfluorohexanoic acid (PFHxA), perfluorodecanoic acid (PFDA), 2,3,3,3-tetrafluoro-2-(heptafluoropropoxy) propanoic acid (GenX), and perfluorobutanesulfonic acid (PFBS). It was found that for PFAS bearing long fluorine-functionalized alkyl chains ($\geq C_4$), the binding affinities were in the range of logK_a = 5.9–6.2. In contrast, much weaker affinities (logK_a = 4.9) were found for TFA (Figure 1d and Figures S3–S10). Figure 1d shows that the binding affinity (logK_a) generally increases with PFAS chain length (TFA < PFBA < PFHxA < PFOA, PFDA). The terminal group also plays a key role—PFBS (sulfonate) exhibits stronger binding than PFOA (carboxylate), likely due to stronger electrostatic interactions. Among the carboxylates, GenX exhibits the highest binding affinity, likely due to secondary interactions involving the ether group. These trends highlight the influence of both chain length and functional groups on PFAS recognition. This finding leads us to suggest that long fluorine-rich chains contribute to the binding by increasing the acidity of the acid group (Table S5) and potential CF–π interactions. The latter interaction is further supported by single-crystal X-ray diffraction studies.

© 2025 Wiley-VCH GmbH

15213773, 2025, 19, Downloaded from https://onlinelibrary.wiley.com/doi/10.1002/anie.202501245 by University Of Texas Libraries, Wiley Online Library on [21/05/2025]. See the Terms and Conditions (https://onlinelibrary.wiley.com/terms-and-conditions) on Wiley Online Library for rules of use; OA articles are governed by the applicable Creative Commons License

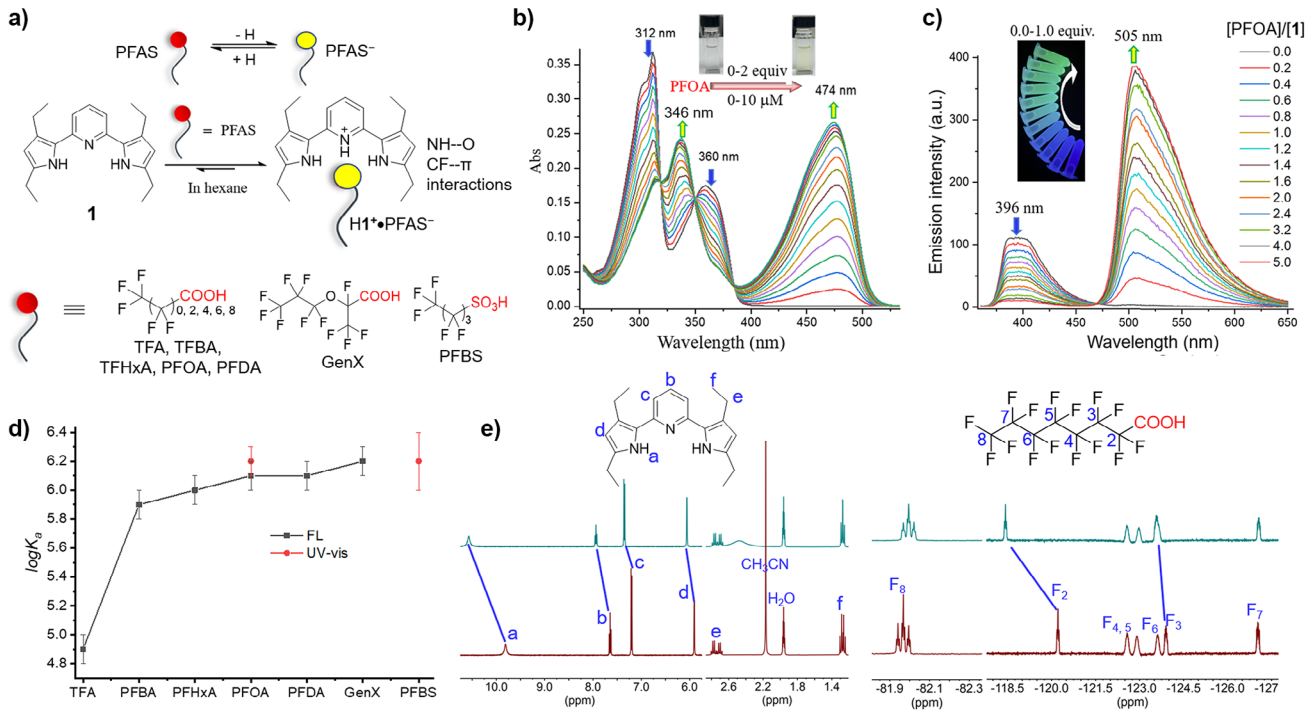

Figure 1. Solution studies between **1** and PFAS. a) Schematic representation of the interaction between **1** and PFAS. b) UV–vis spectra and photographs of **1** (10 μM) with incremental addition of PFOA (0–20 μM) in hexanes (1 cm optical path). c) Fluorescence spectra (hexanes, λ_{ex} = 340 nm, entrance and exit slit width = 5 nm) and photographs (taken under a commercial UV lamp, λ_{ex} = 365 nm) corresponding to the titration of **1** (1.0 μM, 1 cm optical path) with PFOA (0–5.0 μM). d) Binding affinities ($\log K_a$) for the interaction between compound **1** and PFAS in hexanes, determined using the 1:1 binding model from UV–vis and fluorescence spectral titrations (Figures S3–S10), error bars represent the standard deviation from three independent titration experiments. The binding affinity between **1** and PFBS was obtained exclusively through UV–vis titrations, as the complex proved unstable under fluorescence measurement conditions (Figure S11). e) ^{1}H and ^{19}F NMR spectra of compound **1** (5.0 mM) in CD_3CN (bottom) and its mixture with 1 molar equiv of PFOA (top).

Single Crystal Structural Studies

Mixtures containing **1** (5 mM) in the absence or presence of 5 molar equiv of PFAS in CH_2Cl_2/MeOH (1/1, v/v) were prepared and allowed to evaporate at 298 K over the course of 1–2 days. Diffraction-grade single crystals of [**1**•MeOH], [H**1**$^+$•TFA$^-$], [H**1**$^+$•PFBA$^-$•PFBA], and [H**1**$^+$•PFBS$^-$•0.5H_2O] were obtained. These crystals were subjected to X-ray diffraction analyses. The resulting structures are shown in Figure 2, Figures S13–S22, and Tables S1–S2.

Conversion of **1** to its formally positively charged protonated form, H**1**$^+$, in the above complexes was inferred in part based on a shortening of the average pyridine–pyrrole C—C bond (d) within the molecule (d = 1.46(1) Å for **1** vs 1.43(1)–1.44(1) Å for H**1**$^+$). In the single crystal structure of H**1**$^+$•TFA$^-$, hydrogen bonds between the N—H and —COO^- are inferred based on the metric parameters. In the structures of H**1**$^+$•PFBA$^-$ and H**1**$^+$•PFBS$^-$, evidence of CF–π interactions is found in addition to the hydrogen bonds. For instance, a close separation (3.4–3.5(1) Å) between the fluorine (F) atoms and the electron-rich pyrrole subunit in **1** is found. These presumed CF–π interactions provide support for the conclusion drawn above based on the solution phase spectral studies, namely that PFAS with longer fluorine-bearing alkyl chains ($\geq C_4$) bind to **1** more effectively than their smaller congeners (TFA).

Attempts to obtain diffraction-grade crystals of other PFAS species proved unsuccessful in the case of receptor **1**. On the other hand, diffraction-grade single crystals of [H**4**$^+$•PFOA$^-$] were obtained from a solution of **4** (5 mM) in CH_2Cl_2/MeOH (1/1, v/v) that was allowed to evaporate in the presence of 5 molar equiv of PFOA. The resulting crystal structure revealed a binding mode similar to H**1**$^+$•PFBA$^-$.

DFT Calculations

Using the above single crystal data as a starting point, optimized structures of the HOMO and LUMO of **1**, H**1**$^+$•PFOA$^-$, and H**1**$^+$ were calculated, using DFT methods and the Gaussian 09 program.[43] The resulting structures and the energy gap (ΔE) between the HOMO and LUMO are shown in Figure 3 and detailed in Table S3. It was found that the ΔE for both H**1**$^+$•PFOA$^-$ (3.20 eV) and H**1**$^+$ (3.16 eV) are comparable and considerably lower than the corresponding value for **1** (3.98 eV). This finding is consistent with the significant redshift in the UV–vis absorbance and fluorescence emission spectra seen when **1** was titrated with various PFAS. Both the calculated UV–vis absorbance and

© 2025 Wiley-VCH GmbH

15213773, 2025, 19, Downloaded from https://onlinelibrary.wiley.com/doi/10.1002/anie.202501245 by University Of Texas Libraries, Wiley Online Library on [21/05/2025]. See the Terms and Conditions (https://onlinelibrary.wiley.com/terms-and-conditions) on Wiley Online Library for rules of use; OA articles are governed by the applicable Creative Commons License

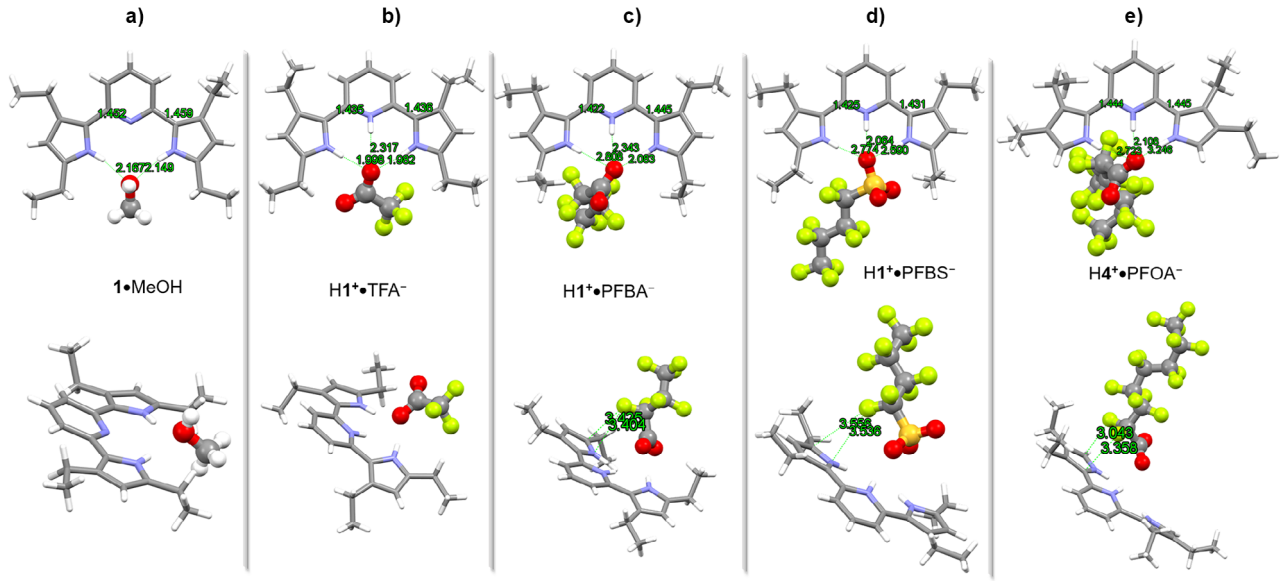

Figure 2. Top and side views of various single crystal structures. a) Free **1** in the form of a methanol solvate and complexes, b) H**1**$^+$•TFA$^-$, c) H**1**$^+$•PFBA$^-$, d) H**1**$^+$•PFBS$^-$, and e) H**4**$^+$•PFOA$^-$ as seen in single crystals of [**1**•MeOH], [H**1**$^+$•TFA$^-$], [H**1**$^+$•PFBA$^-$•PFBA], [H**1**$^+$•PFBS$^-$•0.5H_2O], and [H**4**$^+$•PFOA$^-$], respectively.[42]

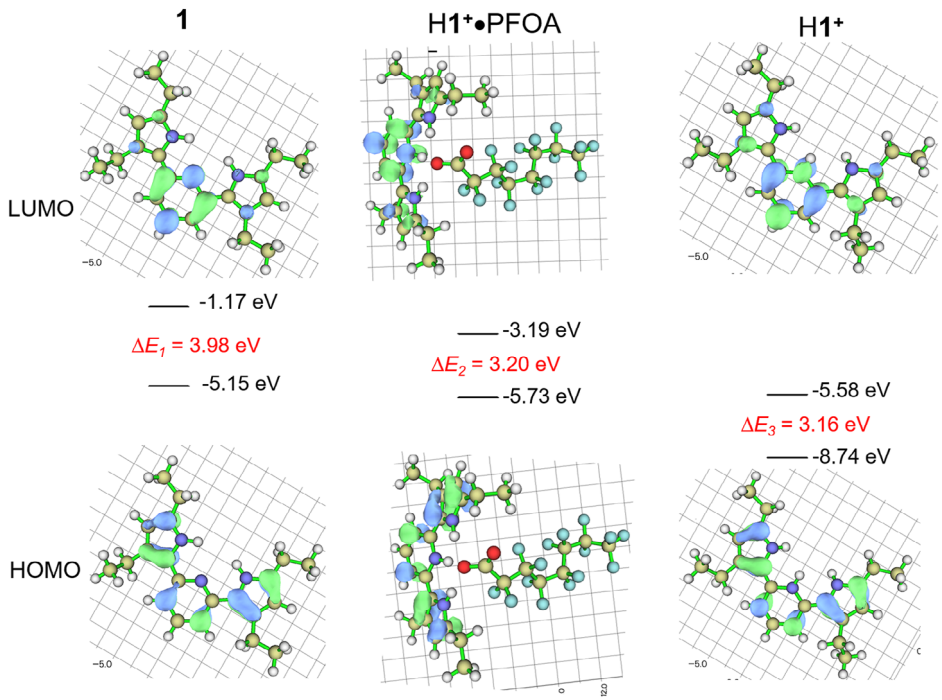

Figure 3. DFT calculations of **1**, H**1**$^+$•PFOA$^-$, and H**1**$^+$. Optimized structures of the HOMO and LUMO, along with the corresponding energies, for **1**, H**1**$^+$•PFOA$^-$, and H**1**$^+$ computed in heptane using DFT methods and the Gaussian 09 program.[42]

fluorescence spectra of **1** and H**1**$^+$•PFOA$^-$ were found to match the experimental spectra (Figure S12).

Fluorescence Emission-Based Detection of PFAS Using 1

The inherent hydrophobic nature and limited solubility of PFAS in water, especially under acidic conditions, along with their strong affinities for **1**, led us to explore an LPE-based sensing strategy wherein a hexanes solution of **1** was used to extract a PFAS analyte from an aqueous source phase. Initial studies were carried out using a solution of **1** (1.0 μM in hexanes) and deionized water solutions (pH adjusted to 2 using HCl) containing various putative contaminants. These separate test solutions included six PFAS (4.0 μM), 500 molar equiv (vs the PFAS) of TFA, *p*-toluene sulfonic acid,

© 2025 Wiley-VCH GmbH

15213773, 2025, 19, Downloaded from https://onlinelibrary.wiley.com/doi/10.1002/anie.202501245 by University Of Texas Libraries, Wiley Online Library on [21/05/2025]. See the Terms and Conditions (https://onlinelibrary.wiley.com/terms-and-conditions) on Wiley Online Library for rules of use; OA articles are governed by the applicable Creative Commons License

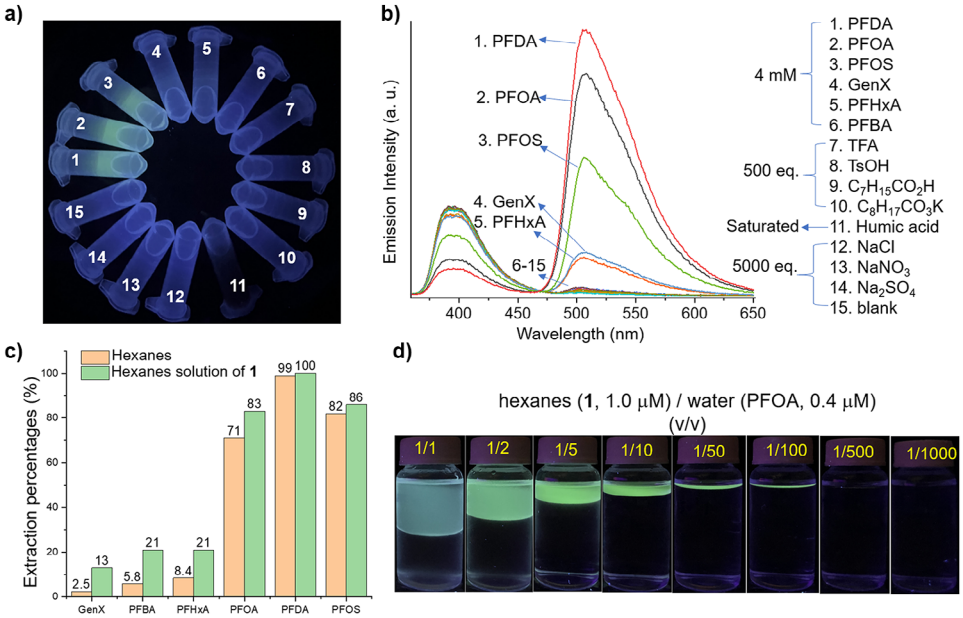

Figure 4. Specific detection of PFAS with **1**. a) Photographs and b) emission spectra of the hexanes layer of **1** (1 mL, 1.0 μM) and various deionized water solutions (1 mL, pH 2) containing various species after shaking and standing for 1 min. c) The bar graph shows the extraction percentage of PFAS (1 mL, 1.0 μM) from an aqueous source phase (pH 2) into hexanes (1 mL) in the presence and absence of **1** (1.0 μM) as determined by LC-MS analyses. d) Photographs of 20 mL of a mixed hexanes solution **1** (1.0 μM) and PFOA (0.4 μM) in water at various volume ratios from 1:1 to 1:1000. The photos were taken after shaking and letting stand for 1 min. All photos were captured using a smartphone under a commercial ultraviolet lamp ($\lambda_{ex} = 365$ nm).

n-octanoic acid, or sodium 1-octanesulfonate. Additionally, potential interferants, including 5000 molar equiv of NaCl, $NaNO_3$, and Na_2SO_4, or strong acids, such as HNO_3, H_2SO_4, and H_3PO_4, were tested, along with saturated humic acid assumed to be present in certain aqueous environments. The process involved mixing the hexanes solution of **1** with aqueous samples (1/1, v/v), followed by shaking and allowing it to stand for 1 min. Only the samples contaminated with PFDA, PFOA, or PFOS exhibited a fluorescent response, which manifested as a change from a blue to yellow–green emission under UV light irradiation (Figure 4a). Further analysis of the fluorescence spectra of the hexanes layer for these mixtures revealed a change in the emission feature around 500 nm in the order PFDA > PFOA > PFOS > GenX > PFHxA > others (Figures 4b and S23). It is noted that sulfonic acids (e.g., PFOS) are more acidic than carboxylic acids (e.g., PFOA) when they have the same chain length and are expected to exhibit stronger binding in hexanes. However, the sensitivity of PFOS is relatively weaker than that of PFOA when using the LPE-based sensing strategy. This is likely due to their higher solubility in the aqueous phase and the stronger hydration of the sulfonic acid moiety relative to a carboxylic acid group.

Liquid chromatography/mass spectrometry (LC-MS) analyses were employed to monitor the PFAS concentrations in the aqueous layer before and after extraction, in the presence and absence of **1**. In all tested samples, the presence of **1** enhanced the extraction of PFAS from the aqueous phase to the hexanes layer. More than 80% of the PFDA, PFOA, and PFOS were extracted into the hexanes solution of **1**, while the extraction levels for the PFAS bearing shorter fluorinated alkyl chains ranged from 13% to 21% (Figure 4c). The greater uptake for the larger systems is ascribed to differences in solubility. In all tested samples, less than 1% of receptor **1** was detected in the aqueous phase (Figure S26).

UV–vis spectral studies involving a range of acids indicate that receptor **1** exhibits a strong response in organic solvents to strong oxyacids such as HNO_3, PFAS, methanesulfonic acid, trifluoromethanesulfonic acid, and *p*-toluenesulfonic acid. (Figure S24). However, the high selectivity of the current LPE method is observed only for longer-chain PFAS, particularly PFOA and PFDA. This suggests that the high selectivity for longer-chain PFAS arises from at least three key factors: The strong binding affinity of receptor **1** for these compounds in hexanes, their low solubility in the aqueous phase, and their relatively weak hydration energies, which collectively facilitate efficient extraction into the hexanes solution and subsequent binding to receptor **1**.

Next, we sought to optimize the sensing conditions and minimize the amount of material used. To this end, 20 mL aliquots of a 1.0 μM hexanes solution of **1** were contacted with 0.4 μM aqueous solutions of PFOA at volume ratios from 1:1 to 1:1000. Using the same conditions as above, through a volume ratio as small as 1/100 a discernible increase in the fluorescent response of the hexanes layer was seen (Figure 4d). These findings are taken as evidence that increasing the total volume of the hexanes/water mixture to hundreds of milliliters, while decreasing the volume ratio to below 1:100 significantly enhances the sensitivity of the system.

© 2025 Wiley-VCH GmbH

15213773, 2025, 19, Downloaded from https://onlinelibrary.wiley.com/doi/10.1002/anie.202501245 by University Of Texas Libraries, Wiley Online Library on [21/05/2025]. See the Terms and Conditions (https://onlinelibrary.wiley.com/terms-and-conditions) on Wiley Online Library for rules of use; OA articles are governed by the applicable Creative Commons License

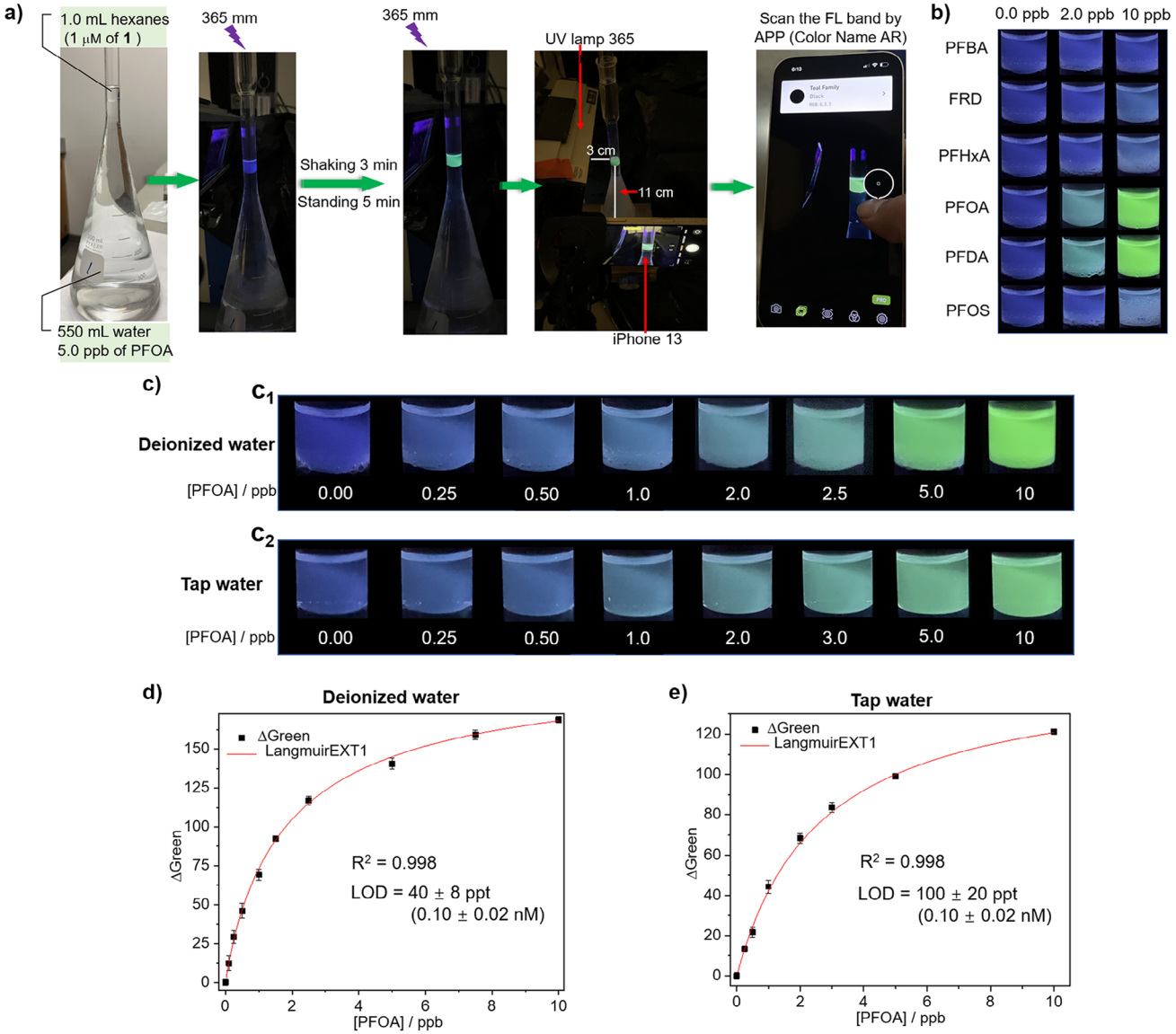

Figure 5. Real-time visual detection of PFAS using receptor **1** under LPE conditions. a) Photographs showing the procedural steps used for the real-time visualized detection of PFOA (5.0 ppb in deionized water) using receptor **1**. b) Photographs highlighting the emission color of the hexanes band containing **1** (1.0 μM) after exposure to PFAS contained in a deionized water source phase. c) Photographs of hexanes solutions of **1** (1.0 μM) were contacted with varying concentrations of PFOA (up to 10 ppb) contained initially in either deionized c_1) or tap c_2) water. d,e), Plots of the changes in the green value of the RGB readout (ΔGreen) as a function of the initial aqueous PFOA concentration in deionized c_1) or tap c_2) water, respectively, as obtained by scanning directly using a color-scanning app and fitting to the Langmuir isotherm. Photos were captured using an iPhone 13 and analyzed with the commercially available Color Name AR app to obtain RGB values.

Real-Time/In Situ Visualization of Ultratrace PFAS Samples

In an effort to detect PFAS at lower concentrations, a special volumetric flask was employed that allowed a 1 mL hexanes solution of **1** (1.0 μM) to be contacted readily with a 550 mL solution of PFAS-containing water. The procedure is shown in Figure 5a. Briefly, a 1.0 mL hexanes solution of **1** (1.0 μM) to 550 mL of deionized water containing the PFAS of interest with the pH adjusted to 2 using HCl. This was followed by shaking for 3 min with 10 s pauses taken at the 30- and 90-s marks to avoid emulsification. After allowing to stand for 5 min to allow for phase separation, the emission color of the hexanes band was captured using a smartphone under ultraviolet illumination using a commercially available lamp with the flask being otherwise protected from light. Efforts to detect six representative PFAS with concentrations of 0.0, 2.0, and 10 ppb are shown in Figure 5b. It was found that only PFOA and PFDA gave rise to significant emission response under these conditions. The relatively weaker response of PFOS at ppb concentrations, compared to its behavior in Figure 4b (PFOS at 4 μM, 2.2 ppm), may be due to changes in its extraction efficiency at different concentrations. Although not ruled out definitively, this specificity leads us to eliminate out simple protonation (as opposed to protonation

© 2025 Wiley-VCH GmbH

15213773, 2025, 19, Downloaded from https://onlinelibrary.wiley.com/doi/10.1002/anie.202501245 by University Of Texas Libraries, Wiley Online Library on [21/05/2025]. See the Terms and Conditions (https://onlinelibrary.wiley.com/terms-and-conditions) on Wiley Online Library for rules of use; OA articles are governed by the applicable Creative Commons License

followed by PFAS counter-anion binding) as the primary sensing mechanism. Another alternative mechanism involving aggregation-induced emission (AIE) strikes us as unlikely given that simple polarity changes involving exposure of **1** to aqueous media do not produce an appreciable fluorescent response. Furthermore, no evidence of aggregation was seen at concentrations of **1** below 2 μM (Figure S25) and all fluorescence-based studies of the interaction between PFOA and **1** were carried out using 1 μM solutions of **1**.

Given the significance of PFOA as a primary PFAS pollutant in the environment, it was chosen for more quantitative analyses. Figure 5c$_1$ shows the emission color changes in the hexanes band upon contact with various aqueous PFOA solutions. Based on these studies, a limit of detection (LOD) as low as 250 ppt (0.6 nM) was determined based on naked-eye observations of the color changes. Utilizing a smartphone color-scanning application ("app") enabled to read out the RGB value of the emissive hexane bond, the changes in the Green Value (ΔGreen) as a function of PFOA concentration could be fitted to a Langmuir isotherm. Applying the $3\sigma/k$ standard employed for LOD calculations involving a linear model,[44] the 3σ value (σ being the standard deviation of the blank) was determined and used as y to calculate the x value (corresponding to the LOD for PFOA) using the Langmuir isotherm equation (Figure S27). The LOD determined in this way was 40 ± 8 ppt or 0.10 ± 0.02 nM.

As the next step in this study, we sought to detect PFAS in samples that more closely resembled those that might be found in the field. With this goal in mind, tests were carried out using the tap water in the Norman Hackerman Building at The University of Texas at Austin. A liquid chromatography/triple quadrupole mass spectrometer (LC/QqQ MS) was used first to quantify the PFAS levels in this tap water. Both the PFOA and PFOS concentrations were found to be below 2.0 ppt. Therefore, a series of PFOA-containing solutions (0.0–10 ppb) were made using 550 mL of laboratory tap water. The pH of all samples was adjusted to 2 using HCl. In addition, 27.5 mg of L-ascorbic acid was added to reduce the Cl_2 that is present in this water. This was done because Cl_2 is able to react with receptor **1** and produce a nonemissive product. All the samples were subject to the LPE-based detection procedures shown in Figure 5a. We found that it was important to follow the shaking procedure as described, namely, pausing and opening the cap to the flask for 10 s at the 30-, 90-, and 180-s marks to release any produced gas. However, a time deviation of up to 10% is acceptable, making this method reproducible and of potential practical use. The total shaking time ensures the complete extraction of PFAS into the small amount of hexanes solution. Pausing and opening the cap helps prevent emulsification, which could interfere with subsequent observations, and ensures safety by allowing any built-up pressure to be released.

Figure 5c$_2$ shows the emission color changes in the hexanes layer produced from the various PFOA-containing tap water samples. Based on these studies, a LOD as low as 250 ppt (0.6 nM) or 100 ± 20 ppt (0.24 ± 0.05 nM) (Figure 5e and Figure S28) could be achieved via naked-eye observation or by using the smartphone color-scanning app, respectively.

Conclusion

In summary, we report here a readily prepared, metal- and fluorine-free PFAS receptor **1**, capable of achieving rapid (within 10 min) and highly sensitive (ppt) real-time visual-based detection of PFOA in aqueous media using a LPE method. Receptor **1** is readily protonated by PFAS to produce an ion pair complex ($H\mathbf{1}^+ \bullet PFAS^-$) and in hexanes displays high binding affinities ($\log K_a$ up to 6.2) for PFAS bearing long fluorinated alkyl chains. PFAS binding results in a strong "turn-on" emission response. A hexanes solution of **1** can efficiently extract long-chain ($\geq C_8$) PFAS from acidic aqueous source phases into the organic layer, allowing for their facile visual-based sensing. The LOD for PFOA contained in either deionized or tap water source phases proved to be as low as 250 ppt under conditions of naked-eye observation. These LOD values could be pushed to 40 ppt for PFOA in deionized water and 100 ppt for tap water, respectively, when the LPE hexanes layer emissive readout was determined using a smartphone color-scanning app. Little interference was produced by shorter PFAS, inorganic, or by the test organic interferants typically present in real-world aqueous samples. We thus suggest that the present approach may have a role to play in field-based detection of PFAS where analytical instrumentation may not be readily available.

Supporting Information

The authors have cited additional references within the Supporting Information.[45–61]

Acknowledgements

This material is based upon work supported by the National Science Foundation under the Center for Aqueous Supramolecular Chemistry, CHE-2420332. (to R.J.H. and J.L.S.). The authors would like to thank the Robert A. Welch Foundation (F-0018 and F-1841 to J.L.S. and G.H., respectively) for support. H.-Y.G. is grateful to the National Natural Science Foundation of China (92156009). X.C. is grateful to the National Natural Science Foundation of China (Grant No. 22271110) and Natural Science Foundation of Hubei Province, China (Grant No. 2022CFA031) for financial support.

Conflict of Interests

The authors declare no conflict of interest.

Data Availability Statement

The data that support the findings of this study are available in the supplementary material of this article.

Keywords: Dipyrrolylpyridines · Fluorescence spectroscopy · Host–guest systems · PFAS · Sensors

© 2025 Wiley-VCH GmbH

15213773, 2025, 19, Downloaded from https://onlinelibrary.wiley.com/doi/10.1002/anie.202501245 by University Of Texas Libraries, Wiley Online Library on [21/05/2025]. See the Terms and Conditions (https://onlinelibrary.wiley.com/terms-and-conditions) on Wiley Online Library for rules of use; OA articles are governed by the applicable Creative Commons License

[1] A. B. Lindstrom, M. J. Strynar, E. L. Libelo, *Environ. Sci. Technol.* **2011**, *45*, 7954.
[2] S. E. Fenton, A. Ducatman, A. Boobis, J. C. DeWitt, C. Lau, C. Ng, J. S. Smith, S. M. Roberts, *Environ. Toxicol. Chem.* **2020**, *40*, 606.
[3] *Technical Fact Sheet: Drinking Water Health Advisories for Four PFAS (PFOA, PFOS, GenX chemicals, and PFBS)*, EPA 822-F-22-002, United States Environmental Protection Agency, Washington, D.C. **2022**.
[4] *Fact Sheet: EPA's Proposal to Limit PFAS in Drinking Water*, United States Environmental Protection Agency, Washington, D.C. **2023**.
[5] C. Ng, I. T. Cousins, J. C. DeWitt, J. Glüge, G. Goldenman, D. Herzke, R. Lohmann, M. Miller, S. Patton, M. Scheringer, X. Trier, Z. Wang, *Environ. Sci. Technol.* **2021**, *55*, 12755.
[6] T. Teymoorian, G. Munoz, S. V. Duy, J. Liu, S. Sauvé, *ACS EST Water* **2023**, *3*, 246.
[7] R. F. Menger, E. Funk, C. S. Henry, T. Borch, *Chem. Eng. J.* **2021**, *417*, 129133.
[8] M. A. Amin, Z. Sobhani, Y. Liu, R. Dharmaraja, S. Chadalavada, R. Naidu, J. M. Chalker, C. Fang, *Environ. Technol. Innov.* **2020**, *19*, 100879.
[9] G. Jiménez-Skrzypek, J. González-Sálamo, J. Hernández-Borges, *J. Chromatogr. Open* **2023**, *4*, 100089.
[10] K. L. Rodriguez, J.-H. Hwang, A. R. Esfahani, A. H. M. A. Sadmani, W. H. Lee, *Micromachines* **2020**, *11*, 667.
[11] Method *537*.1 Determination of Selected Per- and Polyfluorinated Alkyl Substances in Drinking Water by Solid Phase Extraction and Liquid Chromatography/Tandem Mass Spectrometry (LC/MS/MS), United States Environmental Protection Agency, Washington, D.C. **2020**.
[12] H. Niu, S. Wang, Z. Zhou, Y. Ma, X. Ma, Y. Cai, *Anal. Chem.* **2014**, *86*, 4170.
[13] Z. Zheng, H. Yu, W.-C. Geng, X.-Y. Hu, Y.-Y. Wang, Z. Li, Y. Wang, D.-S. Guo, *Nat. Commun.* **2019**, *10*, 5762.
[14] Z. Chen, Y.-L. Lu, L. Wang, J. Xu, J. Zhang, X. Xu, P. Cheng, S. Yang, W. Shi, *J. Am. Chem. Soc.* **2023**, *145*, 260.
[15] Y. Yang, X. Liu, B. Mu, S. Meng, S. Mao, W. Tao, Z. Li, *Biosens. Bioelectron.* **2024**, *257*, 116330.
[16] R. Dalapati, M. Hunter, M. SK, X. Yang, L. Zang, *ACS Appl. Mater. Interfaces* **2024**, *16*, 32344.
[17] A. Concellón, T. M. Swager, *Angew. Chem. Int. Ed.* **2023**, *62*, e202309928.
[18] A. Concellón, J. Castro-Esteban, T. M. Swager, *J. Am. Chem. Soc.* **2023**, *145*, 11420.
[19] S.-N. Lei, H. Cong, *Chin. Chem. Lett.* **2022**, *33*, 1493.
[20] Z. Cheng, H. Dong, J. Liang, F. Zhang, X. Chen, L. Du, K. Tan, *Spectrochim. Acta A Mol. Biomol. Spectrosc.* **2019**, *207*, 262.
[21] Y. He, D. Luo, V. M. Lynch, M. Ahmed, J. L. Sessler, X. Chi, *Chem*. **2023**, *9*, 93.
[22] L. Tian, H. Guo, J. Li, L. Yan, E. Zhu, X. Liu, K. Li, *J. Hazard. Mater.* **2021**, *413*, 125353.
[23] Z. Gou, A. Wang, X. Zhang, Y. Zuo, W. Lin, *Sens. Actuators, B* **2022**, *367*, 132017.
[24] B. Chen, Z. Yang, X. Qu, S. Zheng, D. Yin, H. Fu, *ACS Appl. Mater. Interfaces* **2021**, *13*, 47706.
[25] J. Li, C. Zhang, M. Yin, Z. Zhang, Y. Chen, Q. Deng, S. Wang, *ACS Omega* **2019**, *4*, 15947.
[26] L. Lin, S. Zhou, H. Guo, Y. Chen, S. Lin, L. Yan, K. Li, J. Li, *Microchim. Acta* **2019**, *186*, 380.
[27] E. E. Harrison, M. L. Waters, *Chem. Sci.* **2023**, *14*, 928.
[28] M. H. Hassan, R. Khan, D. Andreescu, S. Shrestha, M. Cotlet, S. Andreescu, *Adv. Funct. Mater.* **2024**, *34*, 2403364.
[29] C. Fang, X. Zhang, Z. Dong, L. Wang, M. Megharaj, R. Naidu, *Chemosphere* **2018**, *191*, 381.
[30] C. Fang, J. Wu, Z. Sobhani, M. Al Amin, Y. Tang, *Anal. Methods* **2019**, *11*, 163.
[31] S. Cho, Y. Kim, *Chem. - Eur. J. 29*, **2023**, e202302897.
[32] Q. Zhang, M. Liao, K. Xiao, K. Zhuang, W. Zheng, Z. Yao, *Sens. Actuators, B* **2022**, *350*, 130851.
[33] C. M. Taylor, M. C. Breadmore, N. L. Kilah, *Sens. Diagn.* **2023**, *2*, 676.
[34] Y. Wang, Y. Chen, Q. Meng, R. Ren, L. Jing, H. Li, L. Zhou, Z. Tian, J. Wang, C. Hou, *Sep. Purif. Technol.* **2024**, *332*, 125824.
[35] C. Hou, F. Chen, D. Cheng, S. Zou, J. Wang, M. Shen, Y. Wang, *Chem. Eng. J.* **2024**, *481*, 148467.
[36] X. Chen, S. Hussain, Y. Tang, X. Chen, S. Zhang, Y. Wang, P. Zhang, R. Gao, S. Wang, Y. Hao, *Sci. Total Environ.* **2023**, *860*, 160467.
[37] F. Caroleo, G. Magna, M. L. Naitana, L. Di Zazzo, R. Martini, F. Pizzoli, M. Muduganti, L. Lvova, F. Mandoj, S. Nardis, M. Stefanelli, C. D. Natale, R. Paolesse, *Sensors* **2022**, *22*, 2649.
[38] H. D. Root, D. N. Mangel, J. T. Brewster, H. Zafar, A. Samia, G. Henkelman, J. L. Sessler, *Chem. Commun.* **2020**, *56*, 9994.
[39] Y. Zhang, D. C. Leary, A. M. Belldina, J. L. Petersen, C. Milsmann, *Inorg. Chem.* **2020**, *59*, 14716.
[40] D. B. Hibbert, P. Thordarson, *Chem. Commun.* **2016**, *52*, 12792.
[41] P. Thordarson, *Chem. Soc. Rev.* **2011**, *40*, 1305.
[42] Deposition CCDC Numbers, 2362284 (for [**1**•MeOH]), 2362281 (for [H**1**$^+$•TFA$^-$]), 2362285 (for [H**1**$^+$•PFBA$^-$•PFBA]), 2362283 (for H**1**$^+$•PFBS$^-$•0.5H_2O]), 2362282 (for [H**4**$^+$•PFOA$^-$]) contain the supplementary crys-tallographic data for this paper. These data are provided freeof charge by the joint Cambridge Crystallographic Data Centre and Fach-informationszentrum Karlsruhe (http://www.ccdc.cam.ac.uk/structures).
[43] M. J. Frisch, G. W. Trucks, H. B. Schlegel, G. E. Scuseria, M. A. Robb, J. R. Cheeseman, G. Scalmani, V. Barone, B. Mennucci, G. A. Petersson, *Gaussian 09, Revision A.1*, Gaussian, Inc., Wallingford, CT, **2009**.
[44] D. MacDougall, W. B. Crummett, *Anal. Chem.* **1980**, *52*, 2242.
[45] G. M. Sheldrick, *Acta Cryst. A.* **2015**, *71*, 3.
[46] A. J. C. Wilson, *International Tables for X-Ray Crystallography*, Vol. C, Tables 4.2.6.8 and 6.1.1.4, Kluwer Academic Press, Dordrecht **1992**.
[47] G. M. Sheldrick, *SHELXTL/PC (Version 5.03)*, Siemens Analytical X-ray Instruments, Inc., Wisconsin, WI **1994**.
[48] A. D. Becke, *J. Chem. Phys.* **1993**, *98*, 5648.
[49] P. J. Hay, W. R. Wadt, *J. Chem. Phys.* **1985**, *82*, 299.
[50] A. W. Ehlers, M. Böhme, S. Dapprich, A. Gobbi, A. Höllwarth, V. Jonas, K. F. Köhler, R. Stegmann, A. Veldkamp, G. Frenking, *Chem. Phys. Lett.* **1993**, *208*, 111.
[51] A. V. Marenich, C. J. Cramer, D. G. Truhlar, *J. Phys. Chem. B* **2009**, *113*, 6378.
[52] Ti. Lu, F. Chen, *J. Comput. Chem.* **2012**, *33*, 580.
[53] T. Lu, *J. Chem. Phys.* **2024**, *161*, 082503.
[54] D. Kalaitzakis, J. D. Rozzell, S. Kambourakis, I. Smonou, *Eur. J. Org. Chem.* **2006**, *2006*, 2309.
[55] E. E. Hardy, K. M. Wyss, M. A. Eddy, A. E. V. Gorden, *Chem. Commun.* **2017**, *53*, 5718.
[56] P. Job, *Ann. Chim.* **1928**, *9*, 113.
[57] BindFit, www.supramolecular.org (accessed: January 2025).
[58] D. B. Hibbert, P. Thordarson, *Chem. Commun.* **2016**, *52*, 12792.
[59] P. Thordarson, *Chem. Soc. Rev.* **2011**, *40*, 1305.
[60] DeepSynthesis, http://isyn.luoszgroup.com/prediction (accessed: March 2025).
[61] S. Liu, Q. Yang, L. Zhang, S. Luo, *Angew. Chem. Int. Ed.* **2025**, e202424069.

Manuscript received: January 15, 2025
Revised manuscript received: March 06, 2025
Accepted manuscript online: March 13, 2025
Version of record online: March 23, 2025

© 2025 Wiley-VCH GmbH

15213773, 2025, 19, Downloaded from https://onlinelibrary.wiley.com/doi/10.1002/anie.202501245 by University Of Texas Libraries, Wiley Online Library on [21/05/2025]. See the Terms and Conditions (https://onlinelibrary.wiley.com/terms-and-conditions) on Wiley Online Library for rules of use; OA articles are governed by the applicable Creative Commons License